

UC Berkeley

UC Berkeley Previously Published Works

Title

Electromechanics of lipid-modulated gating of potassium channels

Permalink

<https://escholarship.org/uc/item/0p98v005>

Journal

Mathematics and Mechanics of Solids, 27(7)

ISSN

1081-2865

Authors

Thomas, Nidhin

Mandadapu, Kranthi K

Agrawal, Ashutosh

Publication Date

2022-07-01

DOI

10.1177/10812865211060071

Copyright Information

This work is made available under the terms of a Creative Commons Attribution-NonCommercial License, available at <https://creativecommons.org/licenses/by-nc/4.0/>

Peer reviewed

Electromechanics of lipid-modulated gating of potassium channels

Nidhin Thomas

Department of Mechanical Engineering, University of Houston, Houston, TX, USA

Kranthi K Mandadapu

Department of Chemical & Biomolecular Engineering, University of California, Berkeley, CA, USA; Chemical Sciences Division, Lawrence Berkeley National Laboratory, CA, USA

Ashutosh Agrawal

Department of Mechanical Engineering, University of Houston, Houston, TX, USA

Abstract

Experimental studies reveal that the anionic lipid phosphatidic acid (POPA), non-phospholipid cholesterol, and cationic lipid DOTAP inhibit the gating of voltage-sensitive potassium (Kv) channels. Here, we develop a continuum electromechanical model to investigate the interaction of these lipids with the ion channel. Our model suggests that: (i) POPA lipids may restrict the vertical motion of the voltage-sensor domain through direct electrostatic interactions; (ii) cholesterol may oppose the radial motion of the pore domain of the channel by increasing the mechanical rigidity of the membrane; and (iii) DOTAP can reduce the effect of electrostatic forces by regulating the dielectric constant at the channel–lipid interface. The electromechanical model predictions for the three lipid types match well with the experimental observations and provide mechanistic insights into lipid-dependent gating of Kv channels.

I. Introduction

Voltage-gated Kv channels play a critical role in the propagation of electrical signals, commonly referred to as action potentials, in neurons [1]. The gating of this channel is regulated by what are called the S4 segments, which carry a number of positive charges. The S4 segments are linked to another critical set of proteins, called the S6 segments, which form the central pore of the channel [2]. A change in the electrochemical potential across the axonal membrane triggers a transmembrane motion of the S4 proteins. This in turn moves the S6 segments, opening the channel and allowing the ions to pass through [3, 4]. While this has been the traditional working model of voltage-sensitive ion channels, experimental studies are now revealing that the channel gating also depends on the lipid composition of the membranes that contain the ion channels [5–9]. For example, in the presence of a negatively charged lipid, called phosphatidic acid (POPA), the electrochemical potential across

Corresponding author:

Ashutosh Agrawal, Department of Mechanical Engineering, University of Houston, Houston, TX 77204, USA.

Email: ashutosh@uh.edu

the membrane required to open the channel increases by ≈ 30 mV [7]. Another lipid, cholesterol, has a much more profound effect. The opening electrochemical potential has been shown to shift by ≈ 160 mV with a small addition of cholesterol in the membrane [6, 9]. Lastly, a positively charged lipid called DOTAP has also been shown to have a similar inhibitory effect on the gating of Kv channels [4, 5, 8].

These different experimental findings lead to a common question. How is this diverse array of lipids able to modulate the gating of Kv channels? While several studies have been conducted to model and comprehend the energetics of protein–protein interactions during the gating of an idealized channel [10–12], specific analysis that would explain the effect of the aforementioned lipids has not been conducted. It is not clear if and to what extent these different lipids could interact and influence the motion of protein segments in the ion channel. It is conceivable that different lipids could potentially interact with distinct domains of the channel and influence the protein kinematics via distinct mechanisms.

In this work, we develop a continuum-scale electromechanical model that accounts for the electrostatic interactions and the elasticity of the membrane to quantify the impact of lipids on channel gating. We use the findings of all-atom molecular dynamics simulations, which reveal that POPA and cholesterol solvate the ion channel by locally aggregating around it [13] and that DOTAP de-solvates the channel, allowing higher water penetration at the channel–lipid interface [14]. While atomistic studies reveal the distribution of lipids around the channel, the mechanisms by which and the extent to which they can regulate the channel gating remains unclear. It is important to test whether the aggregated lipids can alter the energy landscape of the channel–membrane system so as to generate the experimentally observed changes in the gating response of the channels. We note that the shift of ≈ 160 mV induced by cholesterol is significantly larger than the shift of ≈ 30 mV induced by POPA, suggesting that these lipids might be exploiting different mechanisms to regulate the gating. To gain such mechanistic insights, it is necessary to employ a continuum model, owing to the time and length scale limitations of the atomistic studies. However, quantifying the effect of lipids on the gating of a voltage-gated ion channel at the continuum scale is a complex problem, as it requires a coupled electromechanical response of the channel–membrane system. On the one hand, we have the evolving interactions of charges, and on the other hand, we have the mechanical motion of the pore-forming proteins, leading to an elastic deformation of the neighboring membrane. While there are reports of purely mechanical models of gating for a diverse set of channels in the literature [15–20], a combined electromechanical model of channel gating, to our knowledge, does not exist to date.

2. The electromechanical continuum model

2.1. Core features

To predict the consequences of lipid solvation on channel gating, we developed a continuum-scale electromechanical model that captures the essential channel–membrane interactions. We use the experimentally identified channel kinematics to construct a model KvAP channel. Based on atomistic studies, we modify the membrane properties, and predict the consequences on channel configurations and the opening probability of the channel. The main features and assumptions of the continuum model are as follows:

1. The model channel is embedded in the membrane and accounts for the kinematics of the S4 and S6 segments (Figure 1). Studies reveal that the key mechanical motion in a Kv channel is primarily associated with the S4 and S6 segments [3, 21–25]. The gating is initiated by the transmembrane S4 motion regulated by the electrostatic forces, followed by the radial motion of the S6 segments that increases the pore size, allowing the ions to flow across the channel. Figure 1(a) shows the configurations of the S4 and S6 segments in the closed and open states of the channel. Using this discrete picture, we constructed an equivalent model channel, shown in Figure 1(b). Here, S4 is represented as a cylindrical protein (green) and the S6 segments are represented as a hollow cone (teal).
2. A number of competing mechanisms for the motion of the S4 domain are outlined in the literature [3, 4, 4, 26–29]. Inspired by these mechanisms, we assumed that the representative S4 segment undergoes a rigid body translation in the vertical direction and a rotation about the vertical axis passing through the center of the cylinder (Figure 1(b)). The S4 segment configuration, in turn, regulates the positions of the positive charges present on it (red dots in Figure 1(b)). As a consequence, movement of S4 regulates the salt bridge connections that positive charge residues make with the countercharges (negative charges, shown as red dots in Figure 1(b)) present on the nearby protein segments. We assumed that the countercharges remain

stationary during the gating movement, based on the proposed configurations of the protein segments in the open and closed states [3, 21, 22, 24, 31].

3. The pore domain model is based on the known structure and kinematics of the pore-forming S6 segments [21–23, 25, 32]. In the pore domain model, there are assumed to be two domains: one in the outer leaflet of the membrane and the other in the inner leaflet of the membrane (Figure 1(b)). Based on experimental findings [3, 23], we assumed that the outer leaflet domain is a hollow cone that remains stationary during the gating of the channel. The bottom leaflet domain is also a hollow cone but it undergoes configurational changes as the channel transitions between the open and closed states. While the closed structure of the Kv channels is not yet established, the current hypothesized model in the literature assumes that the bottom cone becomes more conical, and that this increases the vertical height and reduces the pore size of the pore domain in the closed configuration [21, 22, 25, 33–35]. We modeled this effective change in the geometry of the bottom domain, as shown in Figure 1(b). Lastly, we assumed that the motion of this bottom domain is rigidly coupled to the motion of the S4 segment via a deformation mapping.
4. As the pore domain transitions between the open and closed states, the surrounding lipids reconfigure to maintain proximity to the pore domain and avoid exposure to the surrounding water. Thus, the gating movement of the pore domain is associated with an energetic cost to remodel the neighboring membrane. To quantify this contribution, we model lipid membrane as a 2D elastic sheet. The midplane of the membrane is assumed to remain flat and the two leaflets are assumed to be kinematically decoupled. The geometry of the membrane at the protein interface is assumed to be regulated by the pore domain geometry. Since the top domain of the pore domain has a fixed conical geometry, the outer leaflet of the membrane does not undergo any remodeling during channel gating (see Figure 1(b)). In contrast, the bottom domain of the pore domain perturbs the orientation and the thickness of the inner leaflet as it transitions between the closed and open states (see Figure 1(b)).
5. The free energy of the system, based on this discussion, comprises the electrostatic energy and the mechanical energy. The electrostatic contributions arise from the transmembrane potential energy, direct electrostatic interactions of the positive charges with the countercharges and the anionic lipids, and self-energy of the charges. The mechanical energy contribution comes from bending and thinning of the membrane. The details of the model are discussed in the following sections.

2.2. Kinematics

The kinematics of the protein segments that regulates the gating of the model channels comprises two key contributions. First is the motion of the S4 segment. It controls the motion of the positive charges within the membrane, thereby regulating the electrostatic interactions. Second is the motion of the S6 segments in the pore domain. It controls the opening of the channel and the deformation of the membrane. These contributions are discussed next in greater detail.

2.2.1. S4 motion. The S4 segment is assumed to be a rigid cylinder representing the alpha-helix state of the protein and is oriented in the vertical direction. Figure 2 shows the side and the top views of the model S4 in the closed and open configurations for the KvAP channel. The radius of the S4 cylinder is considered to be 10 Å, to account for the effective size of the protein. The S4 geometry determines the coordinates of the positive charges. There are five positive residues in the S4 segment, which are distributed along the cylinder as individual charged beads (blue circles in Figure 2). The coordinates of the positive charges are obtained from the molecular structure of the S4 segment. These charges move by 4.5 Å down and rotate by 300° in each helical turn. We model the rotation of S4 about its axis as it undergoes vertical translation. The 3D coordinates of the positive charges are given by

$$x_{\alpha_i} = R_a \cos\left(\frac{\pi}{3} - \frac{\pi\alpha_i}{3} + \omega\right), \quad (1)$$

$$y_{\alpha_i} = R_a \sin\left(\frac{\pi}{3} - \frac{\pi\alpha_i}{3} + \omega\right), \quad (2)$$

and

$$z_{\alpha_i} = z + 4.5\alpha_i, \quad (3)$$

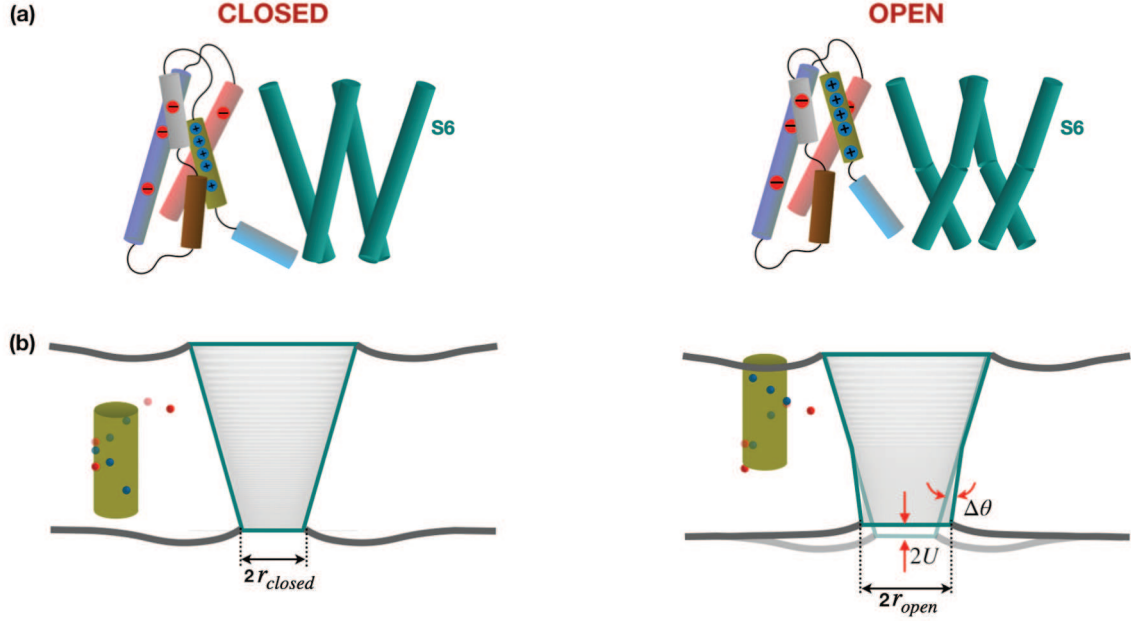


Figure 1. Electromechanical model of Kv channel. Left and right panels show closed and open configurations, respectively. (a) Configuration of the helical segments of the Kv channel (selective segments shown) in the closed and open states used to set up the model channel (motivated by [21–23, 25]). In the closed state, the S4 segment (green) is closer to the inner leaflet and the pore domain segments are tilted with respect to the vertical axis. During opening of the channel, S4 rotates and moves up within the membrane. Concurrently, the inner leaflet segment of the S6 segments (teal) tilt and twist to open the channel. (b) Model Kv channel employed in this study to predict lipid-dependent gating. The model retains the positive charges (blue circles) and the negative charges (red circles) in protein segments. The pore domain is modeled as a hollow cone. The vertical translation of the positive charges changes the electrostatic interactions with the negative charges and the charged lipids. The tilting of the pore domain changes the lipid orientation ($\Delta\theta$) and membrane thickness ($2U$) at the protein interface. The associated electrostatic and mechanical energies regulate the gating of the channel.

where $R_a = 10 \text{ \AA}$ is the radius of the S4 cylinder, α_i corresponds to an index from the set $\{3, 2, 1, 0, -2.33\}$ assigned to the positive charges $\{P1, P2, P3, P4, P5\}$ for the KvAP channel, and ω and z are the parameters used to define the rotation and the translation of the S4 helix. In addition, z is defined as the position of P4 within the membrane; it varies from -9 \AA to 9 \AA to avoid complete exposure of peripheral charges into water. The value of ω varies from 0 to 180° . These assumptions are inspired by the model proposed in [10]. For P5, the (x, y) coordinates are obtained by substituting $\alpha_5 = -1$ and the z coordinate is obtained by substituting $\alpha_5 = -2.33$. While the vertical position of P5 follows the normal alpha-helix rule, the (x, y) position of P5 is not in a standard place because of the kink in the S4 segment. Hence, the adjustment is required to obtain the correct coordinates. We also note that the S4 helix axis is tilted by about 45° with respect to the bilayer normal. However, we suppress the tilt in our model, as S4 side chains are assumed to snorkel into the bilayer–water interface, effectively diminishing the effect of the tilt. The neighboring protein segments contain four countercharges with -1 charge $\{N1, N2, N3, N4\}$. Since these protein segments undergo minimal movement [3, 21, 22, 24, 31], we place these countercharges at fixed locations within the bilayer (red circles in Figure 2). The (x, y, z) coordinates of the countercharges are estimated based on the information of the salt bridge interactions from [24] and are given in Table 1.

2.2.2. Pore domain motion. The S6 segments, which constitute the pore domain, regulate the geometry of the lipids in the vicinity of the channel (Figure 3). We model the projected configuration of the S6 proteins. In the closed configuration, we assume that the S6 segments are oriented at 30° with respect to the vertical axis ($\theta_C^T = \theta_C^B = 30^\circ$), as shown in Figure 3(a). In the open configuration, the protein segments in the inner leaflet are assumed to rotate to 45° ($\theta_O^B = 45^\circ$) (Figure 3(b)). These assumptions are qualitatively based on the findings presented in [21, 22, 25, 33–35]. Based on the hypothesized model proposed in [23], we assume that the protein

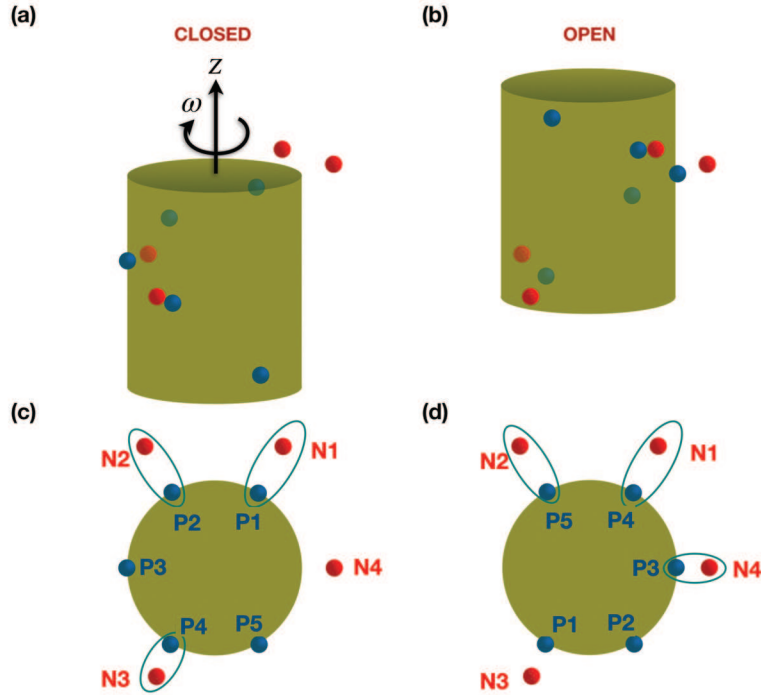


Figure 2. Kinematics and charge distribution of the model KvAP S4 segment. (a, b) Front views of the S4 segment represented as a cylinder (green) in the closed and open configurations, respectively. Positive charges on the S4 are shown as blue spheres and the nearby negative charges are shown as red spheres. The S4 segment rotates by π rad and moves upward within the membrane during the transition from the closed state to the open state. (c, d) Top views corresponding to (a) and (b) showing the salt bridge connections in the closed and open states (blue ellipses).

Table I. Coordinates of negative charges and anionic lipids used in the continuum analysis.

KvAP channel parameters	
Coordinates of N1	(8, 13.59, 12.5) Å
Coordinates of N2	(-9, 14, -4) Å
Coordinates of N3	(-9, -15.0, -7) Å
Coordinates of N4	(13.8, 0, 13) Å
Coordinates of 1st PA lipid in outer leaflet	(-10.72, -9.00, 20) Å
Coordinates of 2nd PA lipid in outer leaflet	(-3.47, -19.70, 20) Å
Coordinates of 1st PA lipid in inner leaflet	(2.48, -13.77, -19) Å
Coordinates of 2nd PA lipid in inner leaflet	(9.92, -8.39, -19) Å
Coordinates of 3rd PA lipid in inner leaflet	(10.0, -17.32, -19) Å

segments in the outer leaflet maintains the same orientation in both the open and the closed configurations. Looking from the top (Figure 3(c) and (d)), each S6 segment is assumed to be oriented at 15° ($\phi_C^T = \phi_C^B = 15^\circ$) with respect to the radial vectors connecting the pore center to the outer leaflet domains of the S6 segment. In the open configuration, the inner leaflet segment is assumed to be twisted to 45° ($\phi_O^B = 45^\circ$) but the twist of the outer leaflet segment is assumed to remain unchanged (based on [23]). We approximate the pore domain as comprising discrete helices with a hollow cone (Figure 3(e) and (f)). In the open configuration, the cone has a kink at the midplane because of the different tilt angles of the S6 segments in the outer and inner leaflets. We note that the protein–membrane interface becomes slightly curved in the open configuration, owing to tilting and twisting of the protein segments (see Figure 3(d)). However, we approximate the interface with straight edges in the model.

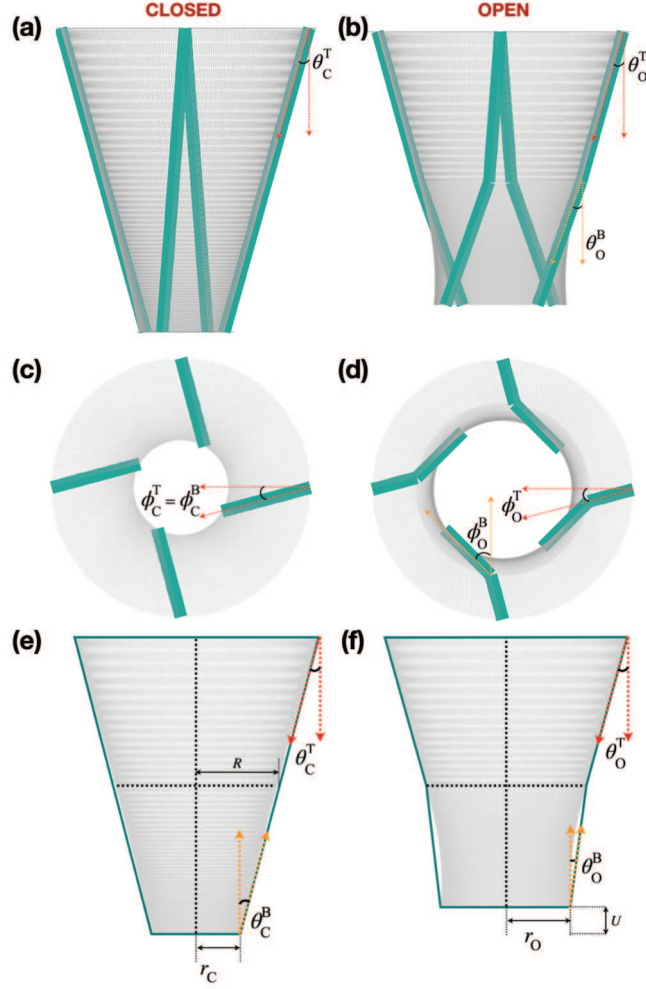


Figure 3. Kinematics of the pore domain in the model channel. **(a, b)** Orientation of four S6 segments in the closed and open configurations (side view). In the closed configuration, S6 segments are assumed to be tilted at 30° with respect to the vertical axis ($\theta_C^T = \theta_C^B = 30^\circ$). In the open configuration, the S6 segment in the inner leaflet is assumed to tilt to 45° ($\theta_O^B = 45^\circ$). The S6 segment in the outer leaflet is assumed to maintain the same tilt. **(c, d)** Top views of the four S6 segments in the closed and open configurations. Each segment is assumed to be oriented at 15° ($\phi_C^T = \phi_C^B = 15^\circ$) with respect to the radial vectors connecting the pore center to the outer leaflet segment. In the open configuration, the outer leaflet segment of the S6 is assumed to remain at ($\phi_O^T = 15^\circ$) but the inner leaflet segment is assumed to twist to 45° ($\phi_O^B = 45^\circ$). These assumptions are qualitatively based on the findings presented in [23, 25]. **(e, f)** The pore domain is modeled as (solid) hollow conical sections in the outer and inner leaflets. The angles of the conical interfaces are obtained from the orientations of the S6 protein segments. In the open configuration, the pore domain has a kink at the midplane because of the different tilts of the S6 segments in the two leaflets. The open configuration also results in the thinning of the inner leaflet.

The motions of the S4 and the S6 segments are linked during the gating of the channel. We therefore link the instantaneous tilt and twist angle associated with the S6 segment to the S4 kinematics through the mappings

$$\theta^B = \theta_C^B + \frac{\theta_O^B - \theta_C^B}{z_O - z_C}(z - z_C), \quad (4)$$

and

$$\phi^B = \phi_C^B + \frac{\phi_O^B - \phi_C^B}{\omega_O - \omega_C}(\omega - \omega_C), \quad (5)$$

where we use $\theta_C^B = 30^\circ$, $\theta_O^B = 45^\circ$, $z_C = -9\text{\AA}$, $z_O = 9\text{\AA}$, $\phi_C^B = 15^\circ$, $\phi_O^B = 45^\circ$, $\omega_C = \pi$, and $\omega_O = 0$ for the KvAP channel.

2.3. Energy contributions in the electromechanical model

The free energy of the total membrane–channel system is given by

$$E = 4E_{\text{Elec}} + E_{\text{Mech}}, \quad (6)$$

where E_{Elec} is the electrostatic energy associated with a single S4 and E_{Mech} is the mechanical energy of the surrounding membrane. A factor of 4 in front of E_{Elec} is incorporated as there are four symmetric repeat units of the S4 and the surrounding countercharges. The electrostatic energy E_{Elec} is composed of four components:

$$E_{\text{Elec}} = E_{\text{Trans}} + E_{\text{SB}} + E_{\text{Lip}} + E_{\text{Self}}. \quad (7)$$

We discuss these contributions in greater detail next.

2.3.1. Transmembrane potential energy (E_{Trans}). The electrostatic energy due to the transmembrane potential arises from the changing vertical positions of the positive residues in a uniform external electric field acting across the membrane. We assume the potential at the interface of the outer leaflet with water to be 0 mV and vary the potential at the interface of the inner leaflet with water from -150 mV to 200 mV. Since the countercharges are fixed, their contribution does not change with the S4 movement and hence is suppressed in the model. We thus write the electrostatic energy due to the transmembrane potential as

$$E_{\text{Trans}}(z_{\alpha_i}, V) = \sum_{i=1}^{i=5} V Q_i f(z_{\alpha_i}), \quad (8)$$

where $f(z_{\alpha_i})$ is given by

$$f(z_{\alpha_i}) = \begin{cases} 1 & z_{\alpha_i} < z_{\text{in}} \\ \left(1 - \frac{z_{\alpha_i} - z_{\text{in}}}{z_{\text{out}} - z_{\text{in}}}\right) & z_{\text{in}} \leq z_{\alpha_i} \leq z_{\text{out}}, \\ 0 & z_{\alpha_i} > z_{\text{out}} \end{cases} \quad (9)$$

and V is the transmembrane potential across the membrane, Q_i is the i th positive charge, z_{α_i} is the vertical position of the i th charge measured from the center of the bilayer (equation (3)), and $z_{\text{in}} = -16\text{\AA}$ and $z_{\text{out}} = 16\text{\AA}$ define the height of the interfaces up to which water is able to penetrate into the two leaflets.

2.3.2. Salt bridge energy (E_{SB}). We obtain the salt bridge's positive charge form in the open and closed states from the atomistic structures. The salt bridge interactions in the open configuration were obtained from [24]. The salt bridge interactions for the closed configuration were obtained from the molecular dynamics simulations of the closed configuration model proposed in [24]. There are three major salt bridge connections in the open and closed configurations (Figure 2 and Table 2). We do not account for the electrostatic interaction between the positive charges as there is no relative movement between them during the gating motions. The salt bridge interaction energy is given by

$$E_{\text{SB}} = \sum_{i=1}^{i=5} \sum_{k=1}^{k=4} \frac{Q_i Q_k}{4\pi\epsilon_0 \bar{D} r_k} \quad (10)$$

where \bar{D} is the average dielectric constant for the salt bridge forming charges, Q_i are the positive charges, Q_k are the countercharges, and r_k is the separation between the salt bridge forming charges (see Table 2).

2.3.3. Protein–anionic lipid interactions (E_{Lip}). We model the electrostatic energy between the clustered anionic lipids in the inner solvation shell and the positive charges similar to the salt bridge energy. The number of anionic

Table 2. Summary of salt bridge interactions.

Salt bridge	State of channel	Distance between charges (Å)
N4-P3	Open	3.64
N1-P4	Open	6.0
N2-P5	Open	6.0
N1-P1	Closed	6.0
N2-P2	Closed	7.21
N3-P4	Closed	4.0

lipids around the S4 and their distance from the positive residues were obtained from our atomistic analysis [13] and are given in Table 1. This interaction energy is computed as

$$E_{\text{Lip}} = \sum_{i=1}^{i=5} \sum_{l=1}^{l=p} \frac{Q_i Q_l}{4\pi \epsilon_0 \bar{D} r_{il}} \quad (11)$$

where p is the number of negatively charged lipid head groups around the protein, Q_l is the charge of the lipid head group, r_{il} is the separation between the charges, and \bar{D} is the average dielectric constant for a positive charge–anionic lipid pair.

2.3.4. Self-energy of the charges (E_{Self}). The self-energy accounts for the energy required to move a charge from one dielectric medium to another. For a bilayer with varying dielectric constant, we use the model proposed in [10] to calculate the self-energy of the positive residues as

$$E_{\text{Self}} = \frac{1}{4} \sum_{i=1}^{i=5} \frac{Q_i^2}{8\pi \epsilon_0 b} \left(\frac{1}{D_m} - \frac{1}{D_w} \right) \left(1 - \tanh \left(\frac{z_{\text{in}} - z_{\alpha_i}}{\lambda} \right) \right) \times \left(1 - \tanh \left(\frac{z_{\alpha_i} - z_{\text{out}}}{\lambda} \right) \right) \quad (12)$$

where $b = 1.8 \text{ \AA}$ is the assumed radius of the charges, and Q_i is the charge.

2.3.5. Dielectric constant. The dielectric constant across the bilayer changes as a function of the distance from the water interface. This variation has been shown to be captured by a hyperbolic tangent function [10]:

$$D = D_w + \left(\frac{1}{4} (D_m - D_w) \left(1 - \tanh \left(\frac{z_{\text{in}} - z}{\lambda} \right) \right) \left(1 - \tanh \left(\frac{z - z_{\text{out}}}{\lambda} \right) \right) \right), \quad (13)$$

where $D_w = 80$ is the dielectric constant of water, $D_m = 14.5$ is the dielectric constant of the lipid membrane assumed in the vicinity of KvAP channel, λ is a length constant that regulates the rate of change of D , $\{z_{\text{in}}, z_{\text{out}}\}$ are the z -coordinates of the water interfaces inside the membrane, and z is the position of the positive or the negative charge. The dielectric constant plot is shown in Figure 4.

2.4. Mechanical energy

The mechanical energy is associated with the bending and the thinning deformations of the membrane and is given by

$$E_{\text{Mech}} = \int_{\Omega'} \left(\frac{K_B}{2} (\nabla^2 u)^2 + \frac{K_A}{2a^2} (u^2) \right) d\Omega, \quad (14)$$

where the first term penalizes the bending deformations and the second term penalizes the thinning deformation of the membrane [18]. In this equation, K_B is the bending modulus, K_A is the compression modulus, $2u$ is the change in membrane thickness, and $2a$ is the resting height of the membrane (see Figure 5; parameter values are listed in Table 3). We have also assumed that the membrane is at zero resting tension.

The variation of equation (14) with respect to u yields the equilibrium equation

$$K_B \nabla^4 u + \frac{K_A}{a^2} u = 0. \quad (15)$$

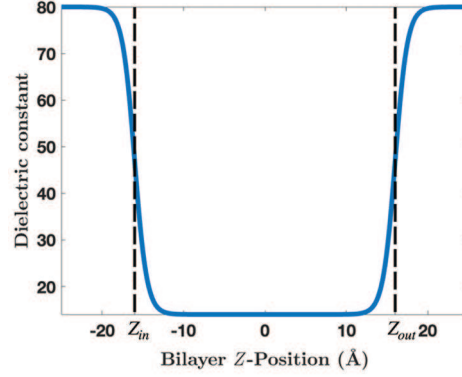


Figure 4. Variation of dielectric constant across the membrane, obtained from equation (13).

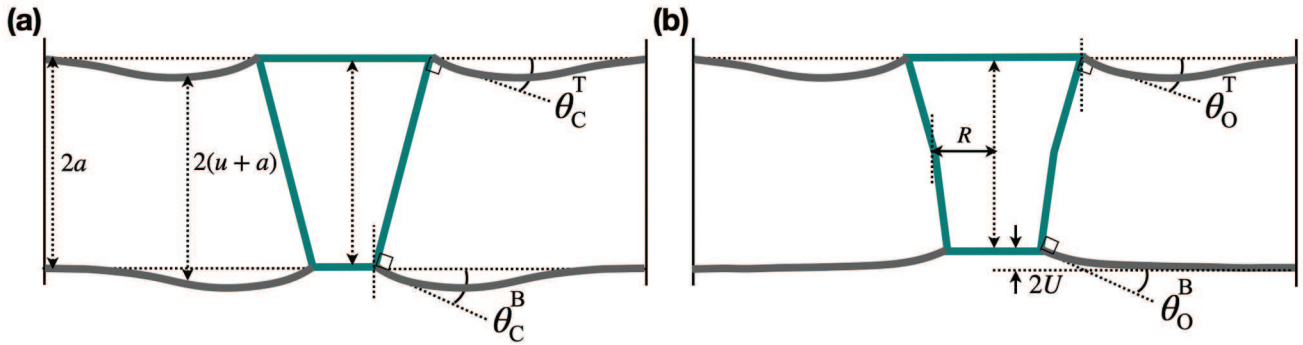


Figure 5. Membrane deformation in the closed and open configurations of the model channel. (a) In the closed configuration, we assume that the projected height of the conical pore domain is equal to the resting thickness of the membrane ($2a = 4$ nm). As a result, $U = 0$. Since the tilt of the conical sections in the outer and inner leaflets are equal, $U' = \frac{1}{2}(\theta_C^T - \theta_C^B) = 0$ in the closed configuration. (b) In the open configuration, $U = -1.835$ Å and $U' = 0.124$ as the conical section in the inner leaflet tilts to $\theta_O^B = 45^\circ$ and twists to $\phi_O^B = 45^\circ$.

Table 3. Parameters used in the continuum model.

Parameter	Value	Source
Dielectric constant of water (D_w)	80	[36]
Dielectric constant of lipids-KvAP (D_l)	14.5	[37, 38]
Radius of S4 (R_a)	10 Å	[10, 13]
Length constant (λ)	1.5 Å	[13]
Inner leaflet interface (Z_{in})	-16 Å	[13]
Outer leaflet interface (Z_{out})	16 Å	[13]
Radius of positive charged residue (b)	1.8 Å	[13]
Monolayer thickness (a)	20 Å	[39]
K_B for POPC system	$27 k_B T$	[39, 40]
K_B for POPC:cholesterol system	$50 k_B T$	[39, 41, 44, 45]
K_A for POPC system	$0.620 k_B T / \text{Å}^2$	[39, 40]
K_A for POPC:cholesterol system	$1.569 k_B T / \text{Å}^2$	[41]

In this equation, we have suppressed the energetic contribution due to the bending of the membrane midplane as it is negligible (it is also shown to be negligible in [18]). Since we require the system to possess cylindrical symmetry, the equilibrium solution is given by the zeroth-order modified Bessel functions of the second kind [18]:

$$u(r) = A_+ K_0(\beta_+ r) + A_- K_0(\beta_- r) \quad (16)$$

where

$$A_{\pm} = -\frac{K_{\mp}U' + \beta_{\mp}UK'_{\mp}}{\beta_{\pm}K'_{\pm}K_{\mp} - \beta_{\mp}K'_{\mp}K_{\pm}}, \quad (17)$$

and r is the radial distance, $2U$ is the thinning of membrane at the membrane–protein interface ($U = u(R)$), U' is the slope of the membrane–protein interface ($U' = \frac{1}{2}(\theta^T - \theta^B)$) in the open and closed states, $\beta_{\pm} = e^{\pm\frac{\pi}{4}}\beta$, $\beta = (K_A/K_B a^2)^{1/4}$, $K_{\pm} = K_0(\beta_{\pm}R)$, and $K'_{\pm} = K'_0(\beta_{\pm}R)$.

As shown in [18], the total energy in equation (14) can be reduced to the boundary integral:

$$E_{\text{Mech}} = \frac{1}{2} \oint_{\partial\Omega'} d\hat{n} \cdot (K_B [\nabla u \nabla^2 u - u \nabla^3 u]). \quad (18)$$

Substituting equation (16) into equation (18), we get

$$E_{\text{Mech}} = \pi R K_B \frac{(\beta_+^2 - \beta_-^2)(K_+U' - \beta_+UK'_+)(K_-U' - \beta_-UK'_-)}{\beta_-K_+K'_- - \beta_+K_-K'_+}, \quad (19)$$

where R is the radius of the protein at the midplane. Substituting the expressions for β_{\pm} , K_{\pm} , and K'_{\pm} , we get

$$E_{\text{Mech}} = \pi R K_B (\sqrt{2}\beta) \left[U^2 + \left(\sqrt{2}\beta + \frac{1}{R} \right) UU' + \left(\beta^2 + \frac{1}{4R^2} + \frac{\beta}{\sqrt{2}R} \right) U^2 \right]. \quad (20)$$

For our calculations, we have considered a bilayer thickness of 4 nm and assumed the projected length of the S6 segments to be 2 nm each in the closed state of the channel. Since the projected length of the S6 segments is equal to the leaflet thicknesses, there is no membrane thinning in the closed configuration and $U = 0$. The headgroup–tail interface of each leaflet is assumed to be perpendicular to the projected S6 segments (see Figure 5). In the closed configuration, the S6 segments are tilted 30° with respect to the vertical axis ($\theta_C^T = \theta_C^B = 30^\circ$ in Figure 3(c)). Since the slopes of both the outer and the inner leaflets are identical at the channel interface, $U' = 0$ in the closed configuration. The twist angle of the S6 segments is assumed to be 15° with respect to the radial vector connecting the center of the pore domain and the outer leaflet end of the S6 segment ($\phi_C^T = \phi_C^B = 15^\circ$ in Figure 3(e)). In the open configuration, the inner leaflet segment of S6 tilts to 45° ($\theta_O^B = 45^\circ$ in Figure 3(d)) and twists to 45° ($\phi_O^B = 45^\circ$ in Figure 3(f)). This results in the thinning of the inner leaflet $U = -1.835 \text{ \AA}$, and a relative change in the slope of the lipids at the channel interface results in $U' = 0.124$. The membrane deformation resulting from the movement of the pore domain is shown in Figure 5.

2.5. Probability distribution

The opening probability of the channel is calculated using a multi-state model given by

$$P_{\text{open}} = \frac{e^{-\frac{E_{\text{open}}}{k_B T}}}{\sum_k e^{-\frac{E_k}{k_B T}}}. \quad (21)$$

where k accounts for all the energy wells in the energy landscape, E_k is the energy of a well, E_{open} is the energy of the well corresponding to the open state, k_B is the Boltzmann constant, and T is the temperature.

3. POPA can regulate the vertical translation of S4 by direct electrostatic interaction

With the model ion channel, we first predicted the consequences of channel solvation by POPA lipids. We model POPA's effect via direct electrostatic interactions with the positive charges in the S4 segment. We do not invoke any POPA-induced changes in the mechanical properties of the membrane as we are not aware of any such findings in the literature. For the POPA-solvated state, we placed one POPA lipid within 1 nm and the other lipid within 1.5 nm from the surface of the S4 helix in the outer leaflet of the membrane, based on our atomistic studies [13]. Since the closed configuration of the ion channel is unavailable to date, we placed two POPA lipids

at a similar distance from the S4 in the inner leaflet as that in the outer leaflet. In addition, we placed an extra POPA lipid within 1 nm, motivated by the fact that the inner leaflet has an additional positive charge.

Figure 6 shows the impact of the POPA lipids on the gating of the model KvAP channel. Figure 6(a) and (b) shows the total energy landscapes for the model KvAP channel in the pure POPC and mixed POPC–POPA membranes, respectively, at 0 mV transmembrane potential as a function of the vertical translation (x -axis) and the azimuthal rotation (y -axis) of the S4 segment. The predicted energy values at the energy wells in $k_B T$ are shown in white text. The rightmost energy well, marked by an arrow, corresponds to the open state of the channel. All the remaining energy wells correspond to the closed state. We compute the energy landscapes at different transmembrane potentials and estimate the opening probability curves (defined in equation (21); these are also referred to as activation curves) for the KvAP channel in pure POPC and POPC–POPA bilayers. Figure 6(c) shows the activation curves for the two systems (pure POPC in gray; POPC–POPA in red). The activation curves for the POPC–POPA bilayer show a rightward shift compared with the pure POPC bilayer curves (red curve in Figure 6(c)). The activation voltages (the voltages at which the opening probability becomes half) for the pure POPC and POPC–POPA bilayers are -30 mV and 1 mV. Thus, POPA solvation leads to a rightward shift of 31 mV.

To understand these trends, we can analyze the energy landscapes in Figure 6(a) and (b). For the pure POPC bilayer, the open state well has the least energy, of $-33.96 k_B T$. As a result, the channel prefers to be in the open state at 0 mV. When POPA solvates the channel, the favorable electrostatic interaction between the POPA and the positive charges in the two leaflets reduces the energies of the wells. The energy of the open state well changes to $-72.04 k_B T$, resulting in a change of $-38.08 k_B T$. By contrast, the energies of the closed state wells undergo a larger reduction (ranging from $-37.78 k_B T$ to $-49.85 k_B T$), as the POPA solvation is stronger in the inner leaflet. So, even though the open state continues to have the least energy, the closed state wells become energetically more favorable. As a result, the channel develops a higher propensity to be in the closed states at 0 mV. This reduced probability of the channel to be in the open state manifests itself in the form of the rightward shift in the activation curve.

The experimental data for the KvAP channel are available for membranes made of three lipids (DOPC, DPhPC, and DPhPC–POPA) [5, 7–9]. While we do not have exact data for the POPC and POPC–POPA membranes, we can expect the channel response to be similar in POPC, DOPC, and DPhPC membranes, for two reasons. First, the POPC membrane has an area compressibility modulus of 255 mN/m, which is comparable to the compressibility modulus, of 265 mN/m, of the DOPC membrane [40, 42, 43]. Second, when we plot the experimental data for the DOPC and DPhPC membranes for the KvAP channel, they show a significant overlap. This indicates that the membrane properties are comparable and that the channel operates in a similar manner in the two membranes. Motivated by these arguments, we overlaid the available experimental data on our predicted curves. Experimental data for the KvAP channel in a DOPC membrane (blue circles) [9], DPhPC membranes (gray and green circles) [7, 8], and a DPhPC–POPA membrane (red circles) [7] are presented in Figure 6(c). Model predictions are in excellent agreement with the experimental data. This suggests that the direct electrostatic interaction between the POPA and the positive charges could be a potential mechanism by which POPA regulates gating of Kv channels.

3.1. Cholesterol can regulate radial movement of pore domain by local membrane stiffening

Next, we estimated the consequences of channel solvation by cholesterol. Studies have shown that cholesterol stiffens POPC or DOPC membranes between 2 and 3 times [39, 41, 44, 45]. Hence, we increased the bending modulus 2 times and the compression modulus 2.5 times (Table 3) to account for the effect of cholesterol solvation. Modeling the change in the elasticity of the membrane, we computed the energy landscapes and the activation curves for the KvAP channel in the presence of cholesterol.

Figure 7(a) and (b) shows the energy landscapes in the pure POPC and POPC–cholesterol membranes, respectively. The open state well has the least energy for the pure POPC membrane system. In the presence of cholesterol, the energy of the open state well increases, making the closed states energetically favorable. This is so because the open state of the channel is associated with a higher compression of the inner leaflet in the protein vicinity. Hence, a cholesterol-rich membrane, with increased stiffness, opposes thinning and makes the open state energetically costlier. As a consequence, the channel develops a higher propensity to be in the closed states. This results in a rightward shift of 155 mV in the activation curve shown in Figure 7(c) (pure POPC in gray curve and POPC–cholesterol in green curve). This prediction agrees well with the experimentally measured shift of 160 mV for the KvAP channel induced by the addition of $\approx 4.0\%$ molar concentration of cholesterol

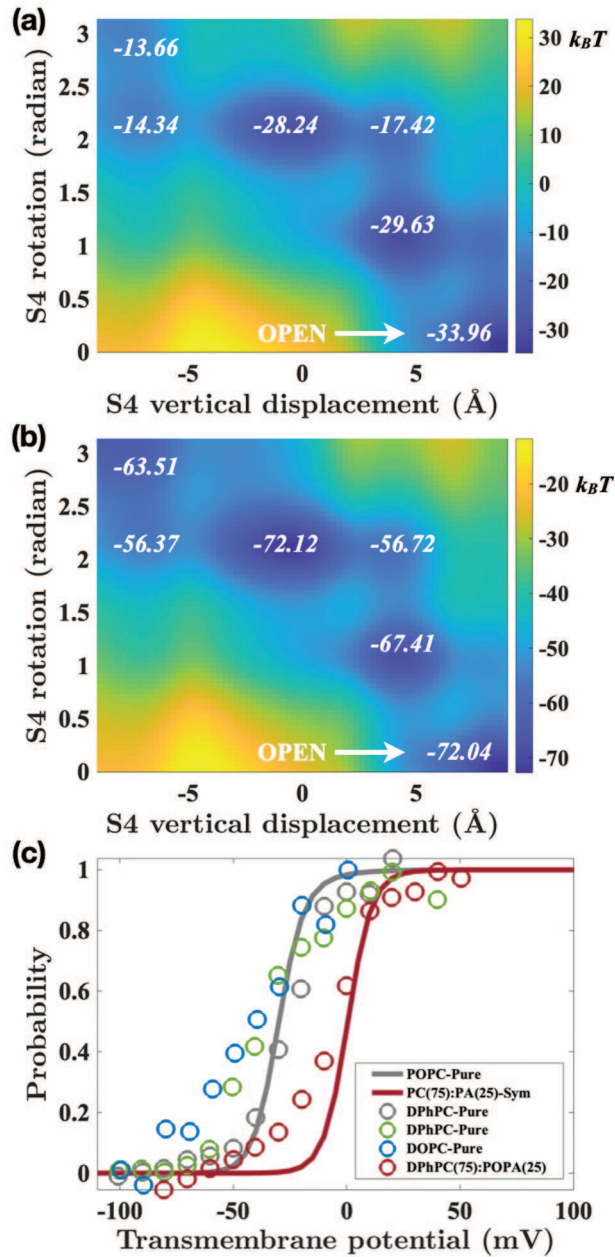


Figure 6. POPA regulates the gating of model Kv channels by direct electrostatic interactions. (a, b) Energy landscapes of the KvAP channel at 0 mV transmembrane potential in pure POPC and mixed POPC–POPA membranes. The vertical position of S4 is on the x -axis, the rotation of S4 is on the y -axis, and the energy values (in $k_B T$) at the wells are in white text. The rightmost well corresponds to the open state of the channel. All other energy wells correspond to the closed states. POPA-positive charge interactions reduce the energies of the wells in (b). (c) Predicted activation curves for the KvAP channel in pure POPC membrane (gray curve) and POPC–POPA membrane (red curve). The presence of POPA creates a rightward shift of 31 mV. Experimental data for KvAP channels in DPhC membranes (gray and green circles) [7, 8], DOPC membranes (blue circles) [9], and DPhC–POPA membranes (red circles) [7] show good agreement with the model predictions. Experimental data are taken from [7–9].

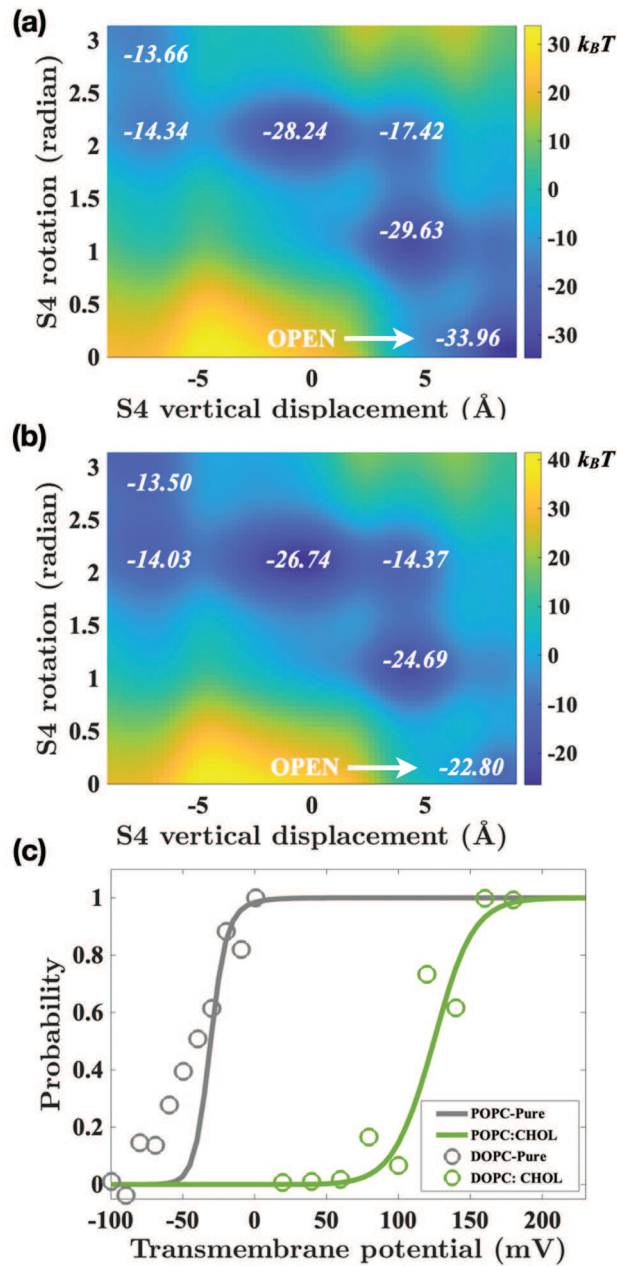


Figure 7. Cholesterol regulates model Kv channel gating by restricting the pore domain motion. (a, b) Energy landscapes of the KvAP channel at 0 mV transmembrane potential in pure POPC and mixed POPC–cholesterol membranes. The vertical position of S4 is on the x -axis, the rotation of S4 is on the y -axis, and the energy values (in $k_B T$) at the wells are in white text. The effect of cholesterol was modeled via increased bending and compression moduli for the mixed POPC–cholesterol membrane. Cholesterol penalizes the open state energy well in (b), owing to increased membrane deformation associated with the open state of the channel. (c) Predicted activation curves for the KvAP channel in POPC membrane (gray curve) [9] and POPC–cholesterol membrane (green curve) [9]. The presence of cholesterol creates a rightward shift of 155 mV. Experimental data for the KvAP channels in DOPC membranes and DOPC–cholesterol membranes are shown in gray and green circles, respectively. The experimental data and the modeling predictions show good agreement. Experimental data are taken from [9].

in a DOPC membrane (pure DOPC in gray circles and DOPC–cholesterol in green circles) [9]. The agreement between the model predictions and the experimental data suggests that the cholesterol-induced changes in the elasticity of the membrane could be a key factor in regulating channel conformation.

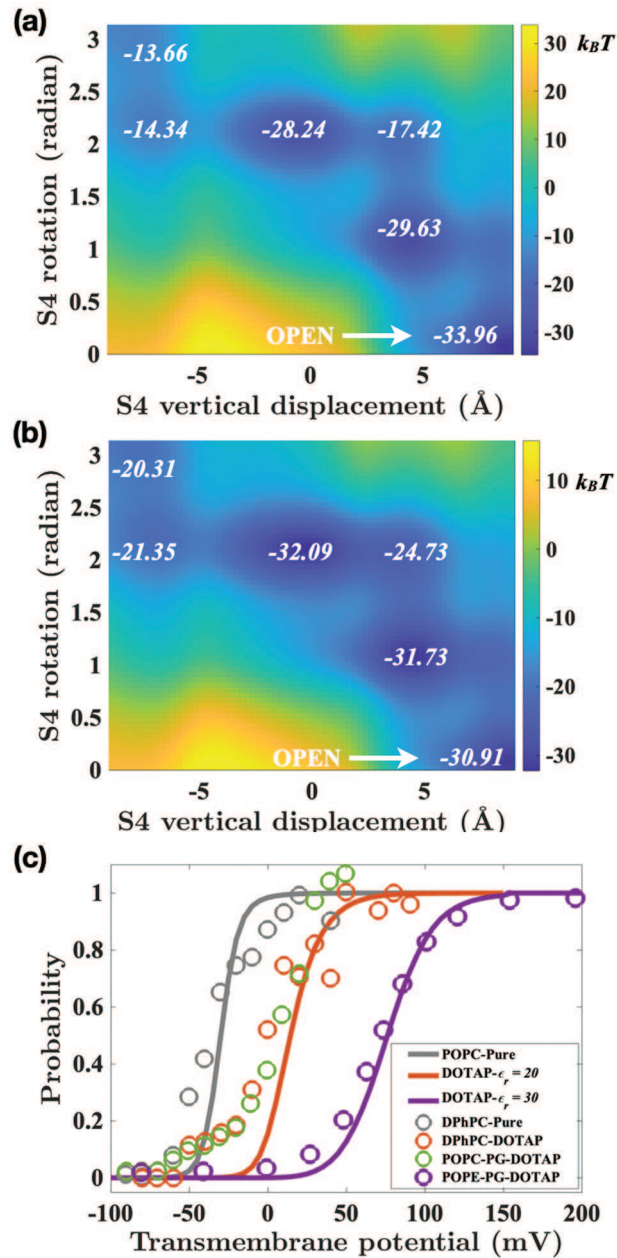


Figure 8. Predicted effect of DOTAP on KvAP gating. **(a, b)** Energy landscapes of the KvAP channel at 0 mV transmembrane potential in pure POPC and mixed POPC–DOTAP membranes. The vertical position of S4 is on the x-axis, the rotation of S4 is on the y-axis, and the energy values (in $k_B T$) at the wells are in white text. We increased the dielectric constant to simulate the effect of DOTAP lipids. This is based on the finding that DOTAP desolvates the S4, triggering increased water penetration in the protein vicinity [14]. As a result, electrostatic interactions diminish and higher depolarization is needed to open the channel. **(c)** Predicted activation curves for the KvAP channel in pure POPC membrane (gray curve) and POPC–DOTAP membranes (red and purple curves). The red and purple curves correspond to dielectric constants of 20 and 30, respectively. Experimental data for DPhC–DOTAP membranes, POPC–PG–DOTAP membranes, and POPE–POPG–DOTAP membranes are shown in red [8], green [5], and purple [4] circles, respectively. Experimental data are taken from [4, 5, 8].

3.2. DOTAP can inhibit KvAP gating by changing the local dielectric constant

Finally, we use our continuum model to investigate the inhibition of KvAP gating [4, 5, 8] by positively charged lipid DOTAP. Molecular dynamics simulations reveal that DOTAP lipids move away from the S4 helix because of the repulsive interactions between the positive charges on the DOTAP and the S4 segment [14]. Furthermore, greater water penetration has been observed in the S4 vicinity [14]. Since DOTAP leads to increased water penetration, we increased the dielectric constant of the lipid–protein interface region in the model. This led to a reduction in the electrostatic interactions between the S4 positive charges and the countercharges. Since the mechanical energy favors the closed states of the channel, a reduction in the electrostatic energy made the closed states relatively energetically more favorable. As a result, a larger depolarization is required to open the channel. Figure 8(a) and (b) shows the energy landscapes for the pure POPC and POPC–DOTAP membranes for the KvAP channel. This results in a rightward shift in the activation curve (Figure 8(c)). Invoking a dielectric constant of 20 (compared with 14.5, used in the prior calculations), the activation curves predicted by the model (pure POPC (gray curve) and POPC–DOTAP (red curve)) match very closely with the measured experimental curves for KvAP channels in DPhPC and POPC–PG–DOTAP membranes (pure DPhPC in gray circles, DPhPC–DOTAP in red circles, POPC–PG–DOTAP in green circles) [5, 8]. The model predicts a rightward shift of 44 mV, which is close to the 38 mV shift observed in experiments [8]. By invoking a dielectric constant of 30, the predicted model curve (purple curve) matches well with the experimental curve obtained for POPE–POPG–DOTAP membranes (purple circles) [4]. The predicted rightward shift of 110 mV matches well with the experimentally observed shift of 107.5 mV.

4. Summary

Phospholipids are essential for the proper gating dynamics of voltage-gated Kv channels. Experimental studies have shown that POPA, cholesterol, and DOTAP inhibit Kv channel gating. Atomistic studies suggest that POPA and cholesterol enter the solvation shell of the ion channel, whereas DOTAP escapes from the solvation shell. We developed an electromechanical model to quantify the extent to which the local distribution of these lipids can alter the energy landscape of the gating of an idealized ion channel. Our analysis suggests that solvated POPA can regulate motion of the S4 segment through direct electrostatic interactions, and that solvated cholesterol can regulate the motion of the pore domain by changing membrane elasticity. The DOTAP lipids, conversely, can alter the local dielectric constant, reduce the electrostatic interactions, and inhibit the gating. For all three lipids, the model predictions match experimental findings. These findings strongly suggest that the channel gating could indeed be regulated by local variations in lipid composition.


Acknowledgements

We acknowledge Dr. Mehdi Torbati for scientific discussions.

Funding

The authors disclosed receipt of the following financial support for the research, authorship, and/or publication of this article: This work was supported by the National Science Foundation (grant numbers CMMI 1562043, CMMI 1727271, and CMMI 1931084) and the Director, Office of Science, Office of Basic Energy Sciences, of the U.S. Department of Energy (contract number DEAC02-05CH11231).

ORCID iD

Ashutosh Agrawal  <https://orcid.org/0000-0002-9923-8603>

References

- [1] Hille, B. *Ion channels of excitable membranes*. Sunderland, MA: Sinauer, 2001.
- [2] Lee, SY, Lee, A, Chen, J, et al. Structure of the KvAP voltage-dependent K⁺ channel and its dependence on the lipid membrane. *Proc Natl Acad Sci USA* 2005; 102(43): 15441–15446.
- [3] Ruta, V, Chen, J, and MacKinnon, R. Calibrated measurement of gating-charge arginine displacement in the KvAP voltage-dependent K⁺ channel. *Cell* 2005; 123(3): 463–475.
- [4] Li, Q, Wanderling, S, Sompornpisut, P, et al. Structural basis of lipid-driven conformational transitions in the KvAP voltage-sensing domain. *Nat Struct Mol Biol* 2014; 21(2): 160.

- [5] Schmidt, D, Jiang, QX, and MacKinnon, R. Phospholipids and the origin of cationic gating charges in voltage sensors. *Nature* 2006; 444(7120): 775.
- [6] Zheng, H, Liu, W, Anderson, LY, et al. Lipid-dependent gating of a voltage-gated potassium channel. *Nat Commun* 2011; 2: 250.
- [7] Hite, RK, Butterwick, JA, and MacKinnon, R. Phosphatidic acid modulation of Kv channel voltage sensor function. *eLife* 2014; 3: e04366.
- [8] Faure, É, Thompson, C, and Blunck, R. Do lipids show state-dependent affinity to the voltage-gated potassium channel KvAP? *J Biol Chem* 2014; 289(23): 16452–16461.
- [9] Jiang, QX. Cholesterol-dependent gating effects on ion channels. *Adv Exp Med Biol* 2019; 1115: 167.
- [10] Lecar, H, Larsson, HP, and Grabe, M. Electrostatic model of S4 motion in voltage-gated ion channels. *Biophys J* 2003; 85(5): 2854–2864.
- [11] Callenberg, KM, Latorraca, NR, and Grabe, M. Membrane bending is critical for the stability of voltage sensor segments in the membrane. *J Gen Physiol* 2012; 140(1): 55–68.
- [12] Grabe, M, Lecar, H, Jan, YN, et al. A quantitative assessment of models for voltage-dependent gating of ion channels. *Proc Natl Acad Sci USA* 2004; 101(51): 17640–17645.
- [13] Thomas, N, Mandadapu, KK, and Agrawal, A. Electromechanics of lipid-modulated gating of Kv channels. *bioRxiv* 2020. DOI: 10.1101/2020.06.12.051482.
- [14] Andersson, M, Freites, JA, Tobias, DJ, et al. Structural dynamics of the S4 voltage-sensor helix in lipid bilayers lacking phosphate groups. *J Phys Chem B* 2011; 115(27): 8732–8738.
- [15] Dan, N, and Safran, S. Effect of lipid characteristics on the structure of transmembrane proteins. *Biophys J* 1998; 75(3): 1410–1414.
- [16] Huang, HW. Deformation free energy of bilayer membrane and its effect on gramicidin channel lifetime. *Biophys J* 1986; 50(6): 1061.
- [17] Wiggins, P, and Phillips, R. Analytic models for mechanotransduction: Gating a mechanosensitive channel. *Proc Natl Acad Sci USA* 2004; 101(12): 4071–4076.
- [18] Wiggins, P, and Phillips, R. Membrane–protein interactions in mechanosensitive channels. *Biophys J* 2005; 88(2): 880–902.
- [19] Haselwandter, CA, and Phillips, R. Connection between oligomeric state and gating characteristics of mechanosensitive ion channels. *PLoS Comput Biol* 2013; 9(5): e1003055.
- [20] Haselwandter, CA and MacKinnon, R. Piezo’s membrane footprint and its contribution to mechanosensitivity. *eLife* 2018; 7: e41968.
- [21] Long, SB, Campbell, EB, and MacKinnon, R. Voltage sensor of Kv1.2: Structural basis of electromechanical coupling. *Science* 2005; 309(5736): 903–908.
- [22] Long, SB, Tao, X, Campbell, EB, et al. Atomic structure of a voltage-dependent K⁺ channel in a lipid membrane-like environment. *Nature* 2007; 450(7168): 376–382.
- [23] Pathak, MM, Yarov-Yarovoy, V, Agarwal, G, et al. Closing in on the resting state of the Shaker K⁺ channel. *Neuron* 2007; 56(1): 124–140.
- [24] Schow, EV, Freites, JA, Gogna, K, et al. Down-state model of the voltage-sensing domain of a potassium channel. *Biophys J* 2010; 98(12): 2857–2866.
- [25] Schow, EV, Freites, JA, Nizkorodov, A, et al. Coupling between the voltage-sensing and pore domains in a voltage-gated potassium channel. *Biochim Biophys Acta, Biomembr* 2012; 1818(7): 1726–1736.
- [26] Larsson, HP, Baker, OS, Dhillon, DS, et al. Transmembrane movement of the Shaker K⁺ channel S4. *Neuron* 1996; 16(2): 387–397.
- [27] Jiang, Y, Ruta, V, Chen, J, et al. The principle of gating charge movement in a voltage-dependent K⁺ channel. *Nature* 2003; 423(6935): 42.
- [28] Chanda, B, Asamoah, OK, Blunck, R, et al. Gating charge displacement in voltage-gated ion channels involves limited transmembrane movement. *Nature* 2005; 436(7052): 852–856.
- [29] Yarov-Yarovoy, V, Baker, D, and Catterall, WA. Voltage sensor conformations in the open and closed states in ROSETTA structural models of K⁺ channels. *Proc Natl Acad Sci USA* 2006; 103(19): 7292–7297.
- [30] Li, Q, Wanderling, S, Paduch, M, et al. Structural mechanism of voltage-dependent gating in an isolated voltage-sensing domain. *Nat Struct Mol Biol* 2014; 21(3): 244.
- [31] Campos, FV, Chanda, B, Roux, B, et al. Two atomic constraints unambiguously position the S4 segment relative to S1 and S2 segments in the closed state of Shaker K channel. *Proc Natl Acad Sci USA* 2007; 104(19): 7904–7909.
- [32] Lee, SY, Banerjee, A, and MacKinnon, R. Two separate interfaces between the voltage sensor and pore are required for the function of voltage-dependent K⁺ channels. *PLoS Biol* 2009; 7(3): e1000047.
- [33] Jiang, Y, Lee, A, Chen, J, et al. X-ray structure of a voltage-dependent K⁺ channel. *Nature* 2003; 423(6935): 33.
- [34] Fowler, PW, and Sansom, MS. The pore of voltage-gated potassium ion channels is strained when closed. *Nature Commun* 2013; 4: 1872.
- [35] Kim, DM, and Nimigean, CM. Voltage-gated potassium channels: A structural examination of selectivity and gating. *Cold Spring Harbor Perspect Biol* 2016; 8(5): a029231.
- [36] Honig, BH, Hubbell, WL, and Flewelling, RF. Electrostatic interactions in membranes and proteins. *Annu Rev Biophys Biophys Chem* 1986; 15(1): 163–193.

- [37] Antosiewicz, J, McCammon, JA, and Gilson, MK. Prediction of pH-dependent properties of proteins. *J Mol Biol* 1994; 238(3): 415–436.
- [38] Spassov, VZ, and Yan, L. A fast and accurate computational approach to protein ionization. *Protein Sci* 2008; 17(11): 1955–1970.
- [39] Doktorova, M, LeVine, MV, Khelashvili, G, et al. A new computational method for membrane compressibility: Bilayer mechanical thickness revisited. *Biophys J* 2019; 116(3): 487–502.
- [40] Venable, RM, Brown, FL, and Pastor, RW. Mechanical properties of lipid bilayers from molecular dynamics simulation. *Chem Phys Lipids* 2015; 192: 60–74.
- [41] Evans, E, Rawicz, W, and Smith, B. Concluding remarks back to the future: Mechanics and thermodynamics of lipid biomembranes. *Faraday Discuss* 2013; 161: 591–611.
- [42] Rawicz, W, Olbrich, K, McIntosh, T, et al. Effect of chain length and unsaturation on elasticity of lipid bilayers. *Biophys J* 2000; 79(1): 328–339.
- [43] Binder, H, and Gawrisch, K. Effect of unsaturated lipid chains on dimensions, molecular order and hydration of membranes. *J Phys Chem B* 2001; 105(49): 12378–12390.
- [44] Rawicz, W, Smith, B, McIntosh, T, et al. Elasticity, strength, and water permeability of bilayers that contain raft microdomain-forming lipids. *Biophys J* 2008; 94(12): 4725–4736.
- [45] Doktorova, M, Harries, D, and Khelashvili, G. Determination of bending rigidity and tilt modulus of lipid membranes from real-space fluctuation analysis of molecular dynamics simulations. *Phys Chem Chem Phys* 2017; 19(25): 16806–16818.